Nonappa, Nonappa; Ikkala, Olli

Hydrogen Bonding Directed Colloidal Self-Assembly of Nanoparticles into 2D Crystals, Capsids, and Supracolloidal Assemblies

Published in:
Advanced Functional Materials

DOI:
10.1002/adfm.201704328

Published: 01/07/2018

Document Version
Peer-reviewed accepted author manuscript, also known as Final accepted manuscript or Post-print

Please cite the original version:
Nonappa, N., & Ikkala, O. (2018). Hydrogen Bonding Directed Colloidal Self-Assembly of Nanoparticles into 2D Crystals, Capsids, and Supracolloidal Assemblies. *Advanced Functional Materials*, *28*(27), 1-14. Article 1704328. https://doi.org/10.1002/adfm.201704328

DOI: 10.1002/ ((please add manuscript number))

Article type: Feature Article

Hydrogen bonding directed colloidal self-assembly of nanoparticles into 2D crystals, capsids, and supracolloidal assemblies

Nonappa and Olli Ikkala

Dr. Nonappa, Prof. O. Ikkala
Department of Applied Physics, Aalto University School of Science, Aalto University, FI-02150, Espoo, Finland.
E-mail: nonappa@aalto.fi olli.ikkala@aalto.fi
Dr. Nonappa, Prof. O. Ikkala
Department of Bioproducts and Biosystems, School of Chemical Engineering, Aalto University, FI-02150, Espoo, Finland,

Keywords: Nanoparticles, supracolloidal self-assembly, hydrogen bonding, capsids, 2D crystals

Abstract: Self-assembly of colloidal building blocks, like metal nanoparticles, is a rapidly progressing research area towards new functional materials. However, in-depth control of the colloidal self-assembly and especially hierarchical self-assembly is difficult due to challenges in controlling the size dispersities, shape/morphology, directionalities, and aggregation tendencies. Using either polydisperse or narrow-size dispersed nanoparticles, considerable progress has been achieved over the past few years. However, absolutely monodisperse nanoparticles could allow new options for rational designs of self-assemblies. Therein, atomically precise monolayer protected nanoclusters ($d < 3$ nm) have recently been synthesized with well-defined metal cores and surface ligands. Their dispersion behaviour is commonly

tuned by surfactant-like ligands. Beyond that, here we deal approaches based on ligand-driven supramolecular interactions and colloidal monodispersity until atomic precision to tune the colloidal self-assembly and hierarchy from nanoscale to mesoscopic scale. Therein colloidal packing to self-assembled 2D crystals and closed virus capsid-inspired shells provide relevant research goals due to ever increasing potential of 2D materials and encapsulation. We will address the hydrogen bonding (H-bonding) directed self-assembly of atomically precise gold and silver nanoparticles and narrow size dispersed cobalt nanoparticles to free-standing 2D colloidal nanosheets, nanowire assemblies, capsid-like colloidal closed shells, as well as higher order structures.

1. Introduction

Simple geometrical packing models in combination of tailored and directional interactions have turned useful for designing and constructing self-assemblies. Therein, controlling the polydispersity of the building blocks has been relevant, and achieving exact monodispersity would, in general, be conceptually the preferred option towards rational designs. So far, supramolecular chemistry has offered a rich variety of approaches towards highly refined supramolecular self-assemblies based on exactly defined low molecular weight molecular building blocks and rationally designed physical interactions using hydrogen or halogen bondings, ionic interactions, metal coordination, and π-stacking. In materials science, exactly defined structures and interactions is rarely accomplished using larger building blocks, such as high molecular weight polymers and, in particular, using colloids. Related to colloidal self-assembly, for example, spontaneous template-free defect-free packing to 2-dimensional (2D) colloidal crystals would be straighforward if the constituent units have exactly similar sizes and if their interacting sites to the neighbouring particles are directional towards the plane, i.e., involve suitable broken symmetry.[1-5] Bending of the 2D sheets from planarity or total suppression of sheet formation can follow even for a minor polydispersity or when defects and geometric frustrations are involved.[6,7] On the other hand, if the constituent units incorporate isotropic interactions, i.e., showing no directionality, 3-dimensional (3D) structures are expected instead of 2D-sheets or closed shells. Therefore, a delicate interplay is foreseen related to the size distribution (exactly monodisperse *vs.* narrow or large polydispersity) and the directionalities of the supramolecular ligand interactions (isotropic *vs.* broken symmetry). Colloidal planar sheets (2D crystals) and closed shells are both expected to be conceptually relevant for 2D materials and encapsulation towards new functions, related hierarchical colloidal self-assemblies.

Within this concept, biological particles such as globular proteins with well-defined shapes (due to protein folding, leading to self-assembly at individual molecular scale) and subsequent directional interactions, can act as subunits to self-assemble into closed shells, i.e., the viral capsids.[8,9] They provide fascinating inspiration for hierarchical self-assembly with exceptional thermodynamic stability. They also follow the principle of genetic economy, efficiency and error-free structure formation using the concept of subunit based self-assembly assisted by a combined electrostatic repulsion, hydrophobic effect and specific interaction between Caspar pairs (i.e. certain aminoacid pairs).[9-11] Importantly, the shape matching proteinic subunits are strictly monodisperse with atomic level precision. Under appropriate conditions, the supramolecular interactions of viral capsid subunits can be tuned to achieve reversible assembly-disassembly and protein engineering can even be utilized to prepare artificial virus particles.[12] Related self-assembly concepts have been widely explored in supramolecular chemistry using molecular level building blocks, dendrimers and block-copolymers where the structure, functional groups and intra- and intermolecular interactions can be controlled to certain precision.[13-15] However, a similar approach using colloidal level building blocks such as inorganic nanoparticles has certain limitations due to challenges in controlling their size, shape, interactions, and stability.[16,17]

The colloidal stability is controlled by a delicate balance between the attractive and repulsive interaction forces between the particles. According to the classical DLVO (Derjaguin-Landau-Verwey-Overbeek) theory, for two identical spherical particles in a dispersion medium, the stability is determined by the sum of the attraction (van der Waals interaction) and the electrostatic repulsion (electrical double layer).[18-20] If the attractive interactions dominate, the particles tend to form random or irreversible aggregates. On the other hand, the dominant repulsive interactions would favor stable colloidal dispersions. The aggregation can also be controlled by screening of the electrical double layer (electrostatic repulsion) using electrolytes or by steric repulsion using (polymeric) brushes (i.e., entropic stabilization). However, when the two particles are closer than a few nanometers (i.e. involving non-DLVO forces such as hydration, hydrophobic and solvation forces), the classical DLVO theory is not applicable.[21,22] Despite these challenges, considerable progress has been made using surface-functionalized colloidal particles, using restricted volume, depleted forces, electrostatic interactions, DNA hybridization, hydrogen bonding (H-bonding), and even the designer inorganic or polymeric patchy particles to control interactions and to achieve higher order assemblies.[23-29] The self-assembly of microparticles using DNA hybridization approach suggested that by tuning the strength of H-bonding (e.g. tuning the DNA melting temperature), it is possible to obtain either random aggregates due to irreversible snapping (i.e. strong H-bonding) or well-ordered macroscopic crystals by H-bonding rearrangement (i.e. weak H-bonding) from micron sized spherical particles.[26]

2. Monolayer protected metal nanoparticles

The pioneering work in 1981 on monodisperse gold 55 (Au_{55}) cluster having triphenyl phosphine (PPh_3) ligands ($Au_{55}(PPh_3)_{12}Cl_6$) initiated the search for ultrasmall nanoparticles with well-defined molecular structures at the atomic level precision, known as nanoclusters.[30] However, the limitations related to the unstable nature of PPh_3 protected nanoclusters warranted further exploration for the preparation of stable ligand-protected nanoparticles.[31] Monolayer protected gold nanoparticles opened a new direction in the synthesis and application of ligand protected noble metal nanoparticles with extraordinary stability.[32] Further, demonstration of ligand exchange allowed the possibilities of mixed ligand shells on nanoparticle surface.[24b,24c,33] Noble metal nanoparticles, especially in the size range <10 nm, have unique optical, magnetic, catalytic as well as potential biological applications.[34] Various approaches have been demonstrated to achieve self-assembled thin films on substrates using partial ligand exchange, layer-by-layer exchange, electrostatic stabilization, DNA base pairing, or complementary hydrogen bonding.[35-46] Similarly, electrostatic assembly of equally sized gold and silver nanoparticles, binary nanoparticle superlattices and virus-nanoparticle hybrid crystals have shown to self-assemble into unprecedented crystal morphologies.[36,39] Among supramolecular interactions, H-bonding is an important non-covalent interaction in controlling the stability, dynamics and hierarchical assembly of biological structures such as proteins and nucleic acids. It is multistimuli responsive (pH, temperature, and solvent), allowing reversible and responsive assemblies. Nanoparticle self-assembly was shown using “brick and mortar” concept by combining nanoparticles containing H-bonding ligand end groups and polymers with complementary H-bonding units.[41] A conceptually simple approach has been shown to achieve assembly of dodecanethiol capped gold nanoparticles using ligand exchange with a few mercaptoundecanoic acid or mercaptohexanoic acid units. The carboxylic acid dimerization led to hexagonally packed array of nanoparticles on surfaces upon solvent evaporation and such H-bonded self-assembled structures possess biomimetic ion-gating properties.[42]

The above studies have been performed using nanoparticles with a finite size dispersities.[41] Note that the phrase "monodispersity" used in nanoscience does actually not always mean exactly defined units. A majority of the so-called “monodisperse” particles in the literature are either polydisperse or with narrow size dispersities. By contrast, there has been a considerable recent progress in the size and shape controlled synthesis and characterization of gold and silver nanoparticles aiming at atomic level precision, an important step in the nanoparticle field.[47-52]

In this feature article the focus will be on the self-assembly of nanoparticles ($d < 10$ nm) decorated with ligands incorporating carboxylic acid peripheral functionalities. Carboxylic acids are particularly attractive therein for several reasons: 1) They allow H-bonding interactions between ligands of neighbouring nanoparticles due to carboxylic acid dimerizations as a supramolecular motif; 2) In constructing ditopic ligands with opposing carboxylic and metal binding group (-SH, and $-NH_2$) as separated by a spacer (see **Figure 1a,e**), the carboxylic acids interestingly do not interfere the metal binding. We point out that selecting the peripheral supramolecular binding motifs is untrivial, as most of the generally used supramolecular binding motifs could also bind to metals, thus leaving carboxylic acids one of the few feasible ones; 3) Finally, carboxylic acids can be converted to their salt form under basic conditions, thus facilitating water dispersibility and balance of the H-bonding and ionic interactions. Special emphasis in this feature article is by *para*-mercaptobenzoic acid (*p*MBA) and *para*-aminobenzoic acid (*p*ABA) ligands. They will be used as ligands for H-bond directed self-assembly of atomically precise gold nanocluster (Au_{102}-*p*MBA_{44}) and silver nanocluster (Ag_{44}-*p*MBA_{30}) (Figure 1b,c and later **Figures 2 and 3)**, in both cases involving a fraction of the carboxylic acid in the salt from. A comparison is made to a polydispersed cobalt nanoparticles (Co-*p*ABA) having size $d < 8$ nm (Figure 1d and later **Figure 7**). We will first describe the self-assembly strictly monodisperse gold nanoclusters to 2D colloidal crystals driven by H-bonds with broken symmetry. Next, we will describe bending and closing of the sheets to spherical capsids having monolayer and a few layer thick shells. Further we will describe how hydrogen bonded nanoclusters can be used to direct self-assemblies of nanowires. Finally, we also disclose our results on two types of colloidal capsids, *viz* ellipsoidal capsids with monolayer thick shell and cylindrical capsids composed of a few layered shell from cobalt nanoparticle self-assembly.

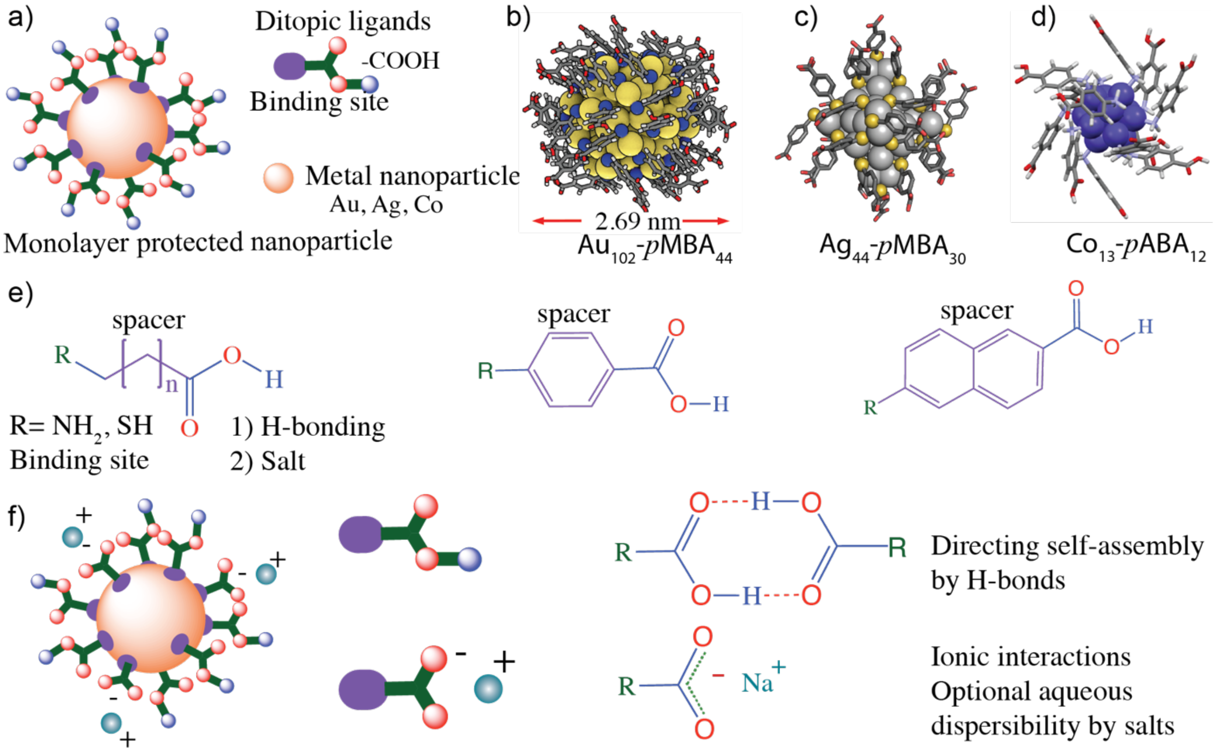

Figure 1. Nanoparticle building blocks and chemical structures of ligands discussed in this feature article. a) Schematic representation of monolayer protected metal nanoparticles using ditopic ligands with a metal-binding and carboxylic acid ends. b) X-ray single crystal structure of the gold nanocluster Au$_{102}$-*p*MBA$_{44}$ incorporating *p*-mercaptobenzoic acid ligands (*p*MBA). Reproduced with permission from ref[68]. © 2017 WILEY-VCH Verlag GmbH & Co. KGaA, Weinheim. c) X-ray single crystal structure of the silver nanocluster Ag$_{44}$-*p*MBA$_{30}$. (H-atoms are not shown for clarity). Reproduced with permission from ref[69]. © 2013 Macmillan Publishers Limited. d) Suggested Co$_{13}$-*p*ABA$_{12}$ (*p*ABA = *p*-aminobenzoic acid) cluster based on computational modelling. Reproduced with permission from ref[76]. © 2017 WILEY-VCH Verlag GmbH & Co. KGaA, Weinheim. e) The chemical structures of the present ditopic ligands, showing the metal binding units (R), spacers, as well as the carboxylic acid group. f) The versatility of the carboxylic acid peripheral functional group to act a H-bond directing unit due to carboxylic acid dimerization (in the protonated state) and water dispersion promoter (in the salt form).

3. Atomically precise nanoclusters

Atomically precise nanoclusters ($d < 3$ nm) contain well defined molecular structures with exact number of metal atoms and surface ligands. The structure of nanoclusters is determined using single crystal X-ray diffraction, cryogenic transmission electron microscopy (Cryo-TEM), or mass spectrometry.[47,50,51] The concept of comparing inorganic nanoparticles to protein mimics has already been proposed in the literature,[53] however, the lack of 3D structural details of such plasmonic nanoparticles remained a hurdle in providing detailed mechanistic insights. In this context, the self-assembly of atomically precise quantum sized nanoclusters with inherent structural complexity,[50] and well-defined structure, the location and orientation of the surface ligands will be vital in enhancing the current understanding on nanoparticle self-assembly. The self-assembly of atomically precise nanoclusters, typically having the core diameter from subnanometer to 2-3 nm, will be of particular interest due to the well-defined size, as they provide a link between molecule-like simple organometallic complexes and plasmonic nanoparticles.[48,49] This small size induces energy quantization due to quantum confinement in the extremely small size.[54] Therefore, remarkably different physical and chemical properties are displayed by nanoclusters having application potential in the new sensors, photography, biology, and optoelectronics. Unlike large plasmonic nanoparticles, where the surface plasmon resonance is due to collective excitation, the nanoclusters show molecule like multiple bands in their electronic spectra.[54] The properties such as non-metallic and metallic characters can be tuned by changing the size of the nanoclusters.[54] The fundamental requirements are the shape and composition of the metal core and ligand structure. The core determines the electronic and optical properties and the ligand engineering allows tuning of the chemical properties and packing. However, achieving higher order structures using nanocluster self-assembly is a challenging task as the inter-nanocluster interactions (electrostatic and dipolar van der Waals interactions) are comparable to the thermal fluctuation energy of the environment, thereby complicating the formation of higher order structures unlike plasmonic nanoparticles.

4. Self-assembled 2D colloidal nanosheets

In materials science, the two-dimensional structures of a single or a few layer thicknesses using atomic, molecular, or nanoscale units have received tremendous attention since the exfoliation of graphene.[55,1-5] Graphene is an unique example, as it is a component of graphite, which consists of 2D stacks of graphene in its bulk (3D) crystals. The 2D layered graphene exhibits excellent charge carrier mobility, mechanical properties, optical transparency and electronic properties making it suitable for novel functional devices.[56] Similarly, other ultrathin 2D nanomaterials have unique material properties due to high surface area and quantum confinement of electrons in two dimensions and have been demonstrated to improve the performances of batteriess, catalysts, solar cells and act as reinforcing components in nanocomposites.[57] More importantly, the structures allow studies of anisotropic or dimension-dependent physical and chemical properties which might pave way for novel materials with unanticipated properties. Various approaches such as exfoliation, molecular beam epitaxy and solution phase synthesis have been used to achieve 2D nanostructures, including protein engineering for dynamic flexible 2D biocrystals.[56-64] Such layered structures display anisotropic growth and interactions due to strong lateral bonding and weak van der Waals interaction between the layers (in graphene) or other supramolecular interactions. Recently 2D polymers and supramolecular polymers have been demonstrated using photopolymerization techniques.[65,66] However, when it comes to metals and colloids, they have a tendency to form bonding to form 3D structures, which limits the spontaneous access to 2D layered colloidal structures in template-free manner.

In material science, the ligand protected 2D colloidal crystals are of great interest, e.g., due to the electron transport phenomena.[67] It has been shown that in 2D arrays, the transport occurs through hopping process and the presence of ligands on the surface might provide a tunneling barrier. The conductivity can be tuned by controlling the hopping steps. In metal oxide nanosheets, the transport can be improved by ligand passivation.[60] Further, unlike individual larger spherical nanoparticles, 2D materials show strong quantum confinement in the in-plane direction. Related to nanocluster based 2D materials, nanosheets derived from CdSe nanocrystals and other related quantum dots have been reported and reviewed.[63] However, a majority of the nanosheets are prepared by growth control using molecular precursors. Nanosheets or 2D colloidal crystals of thickness below 5 nm can also be achieved using the concept of colloidal self-assembly. In self-assembly, the feasible building blocks are foreseen to be well-defined monolayer protected nanoparticles which pack into sheets through supramolecular interactions between the ligands. Ligand mediated self-assembly would allow highly ordered array up to mesoscopic length scale and simultaneously prevent or control the electronic coupling between the nanoparticles, thereby retaining the intrinsic material properties of individual nanoparticles. Here, as an example, we discuss the self-assembled 2D colloidal sheets from water dispersible atomically precise gold nanocluster Au_{102}-*p*MBA_{44} (Figure 2).[68] The nanocluster contains 102 gold (Au) atoms and monolayer ligand shell of 44 *p*MBA molecules, with carboxylic acids facing the periphery. The nanocluster with the core diameter of 1.59 nm and overall size of 2.7 nm represents the first nanocluster which has been completely characterized using single crystal X-ray diffraction (Figure 1b).[47] The space filling model in its solid state can be compared to the size of a fully folded 26 kDa protein molecule, a colloidal subunit. The solid is stable under ambient conditions. The nanocluster has been shown to possess similar structure also in its solution state.[51] It is soluble in methanol in its protonated state but insoluble in water.[47] However, partial deprotonation of the surface carboxylic groups leads to patchy water dispersible clusters which are insoluble in methanol. This property has been utilized to grow single crystals for X-ray diffraction using 46% aqueous methanol in the presence of sodium chloride and sodium acetate at pH 2.5.[47] Interestingly, a closer look at the distribution of the ligands reveals that there is a preferential orientation towards the equatorial plane, i.e., to form anisotropic patches (Figure 2d-2f).

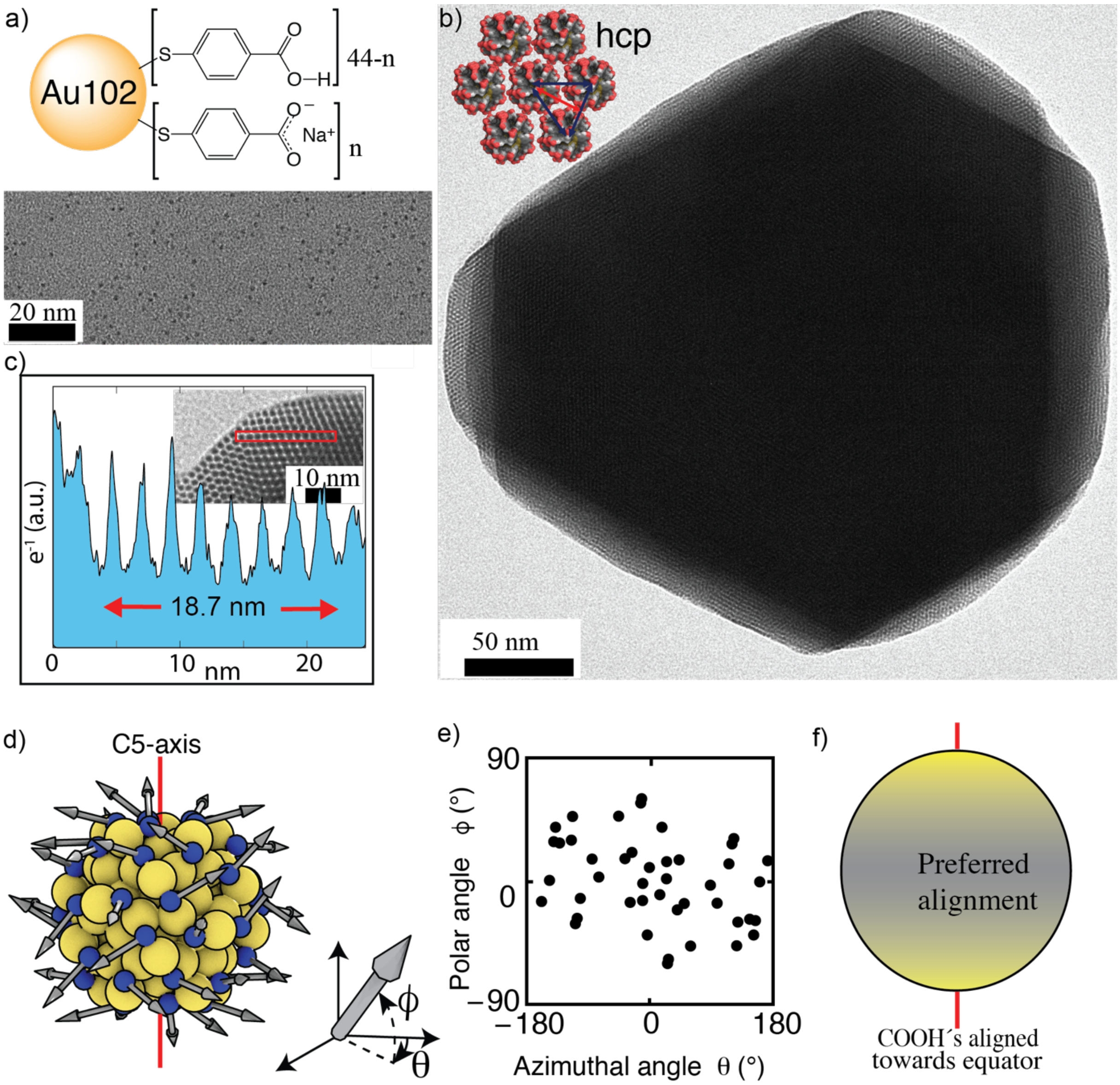

Figure 2. Self-assembled template-free 2D colloidal nanosheets. a) TEM micrograph of aqueous dispersed Au_{102}-*p*MBA$_{44}$, when a fraction of the total 44 *p*MBA ligands is in the salt form. b-c) Upon controlled (slow) solvent exchange from water to methanol by dialysis, 2D colloidal nanosheets are spontaneously formed as shown by TEM micrograph. It shows facetted one nanoparticle thick hexagonally close packed (hcp) sheets. The TEM image shows that three of them are partially stacked in this case. d-e) Orientation and distribution of ligand and H-bonding patches showing a preferential anisotropic distribution at the equatorial plane.

Reproduced with permission from ref[68]. © 2016 WILEY-VCH Verlag GmbH & Co. KGaA, Weinheim.

This raises a question, whether anisotropic growth of self-assembled structures in 2D is possible by breaking the (3D) symmetry? Recently it was achieved using partially deprotonated nanoclusters Au_{102}-*p*MBA_{44}.[68] The partial deprotonation of the carboxylic acids to sodium salts using aqueous sodium hydroxide provide access to both H-bonding due to protonated COOH groups as well as electrostatic repulsion due to negatively charged carboxylates COO^-, allowing aqueous dispersibility. Upon controlled dialysis of aqueous dispersion against methanol, the nanoclusters underwent hexagonally packed 2D colloidal nanosheets (Figure 2b) with monolayer thickness, representing the first controlled and free-standing 2D crystals from atomically precise nanoclusters using supramolecularly controlled template-free self-assembly. The TEM analysis showed hexagonally close packed structures with a periodicity of 2.3 nm and inter-nanoparticle distance of 2.7 nm (Figure 2c) with facetted edges (Figure 2b). This can be explained because the deprotonation to Na-salts provides electrostatic repulsion and the protonated carboxylic acid groups undergo H-bonding dimerization. Therefore, a delicate balance between attractive and repulsive interactions is maintained. The equatorial distribution of the H-bonding patches provides a strong lateral binding (intralayer direction) and the interaction between the layers (inter-layer) of nanosheets will be weak π-stacking between the surface ligands as it was also shown in the crystal structures.[47] Therefore, this structure is reminescent to graphene, but in this case due to colloidal units and supramolecular bonds. However, the packing pattern in the 3D X-ray single crystal structure[47] has been shown to be different than in the present 2D-case and no hexagonal patterns were observed in the 3D crystal packing. Therefore, the self-assembly of the present 2D colloidal crystals and the previously reported 3D single crystal formation follow a significantly different path. However, continuing the dialysis led to the formation of stacked sheets into bundled structures (see Figure 2b showing 3 sheets stacked).[68] This is in analogy with the 2D crystal formation in keplerates (see later) and apoferritin particles, driven by the anisotropic distribution of the interacting patches.[5]

Another extensively studied system is silver nanocluster Ag_{44}-*p*MBA_{30}. The nanocluster is composed of 44 silver (Ag) atoms and 30 *p*-mercaptobenozic acid (*p*MBA) units, with overall size of 2.5 nm and molecular weight of ~10 kDa (Figure 1c).[69,70] Based on mass spectrometry analysis and single crystal X-ray diffraction studies, it has been shown that all the carboxylic acids exist in their fully protonated form. However, the nanocluster carry -4 charge, which comes from the metal core and not from the carboxylates.[69] These negative charges are stabilized by counter cations, therefore, represented as M_4-Ag_{44}-*p*MBA_{30} (where, M=Na). The extraordinary stability of Na_4-Ag_{44}-*p*MBA_{30} nanoclusters and the possibility to provide even semi large-scale synthesis up to 140 g (i.e. three orders of magnitutue higher than typical nanoparticle synthesis) has encouraged extensive investigation for various applications. The nanoclusters self-assemble into rhombus shape crystals in the solid state. Considering the 3D crystals, unlike the gold nanocluster Au_{102}-*p*MBA_{44} discussed earlier, the crystal structure of Na_4-Ag_{44}-*p*MBA_{30} displays a hexagonally arranged superlattice, mediated by inter-nanoparticle hydrogen bondings (**Figure 3**).[69] The ligands are classified into two types based on their H-bondings, i.e., twofold or double bundles (L2) and three-fold or triple bundles (L3). In the solid state, each double bundle (L2) contributes to the two H-bonding dimerizations between the neighbouring nanoclusters, whereas each triple bundle (L3) contributes to three inter-nanocluster H-bonding dimerization.

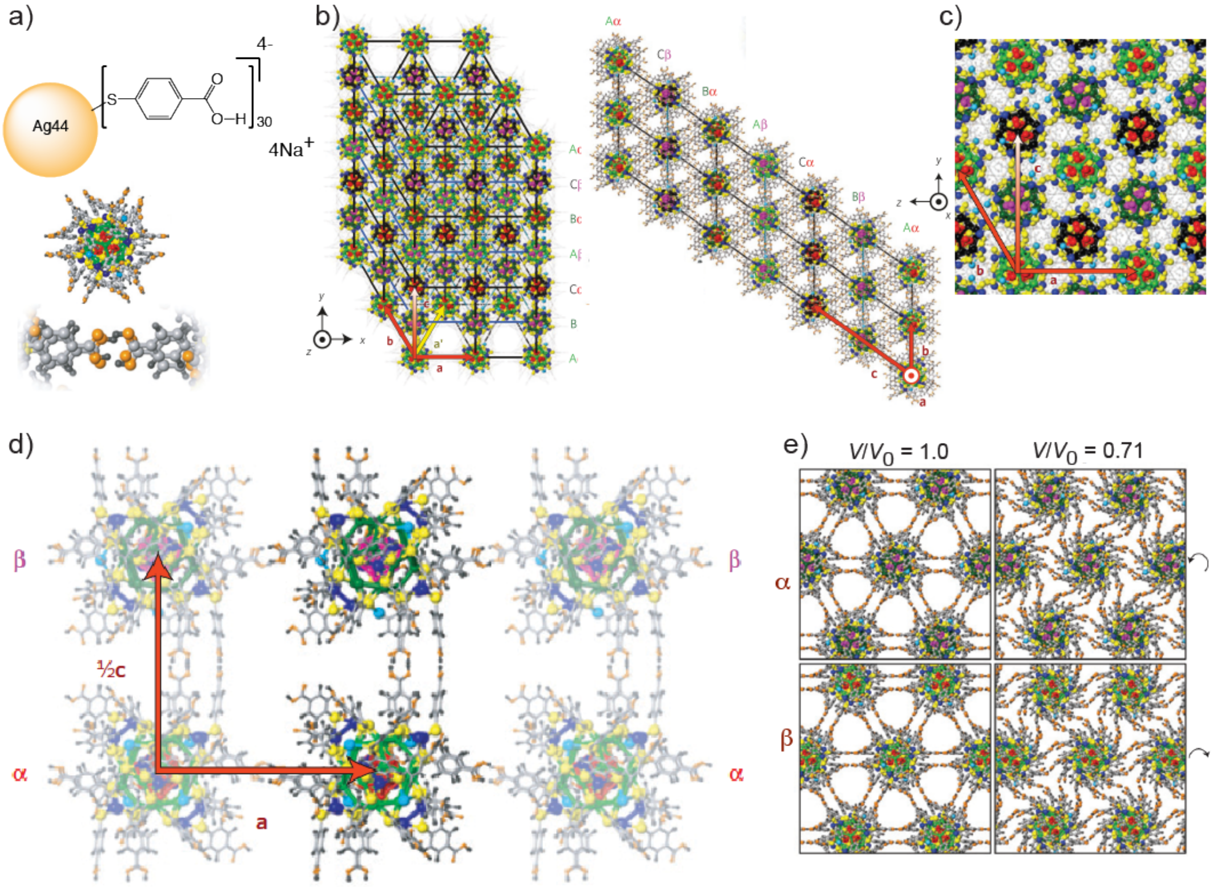

Figure 3. H-bonding in Na_4-Ag_{44}-*p*MBA_{30} nanoclusters. a) Chemical structure, single crystal X-ray structure of single Na_4-Ag_{44}-*p*MBA_{30}, and H-bonding due to carboxylic acid dimerization. b, c) Inter and intra-layer H-bonded structures with hexagonal packing in 3D and 2D views. d) A close-up view showing inter-layer H-bonding. e) Rotational structural transition of two layers showing ligand flexure and rotation of nanoclusters. The nanoclusters in the two different planes rotate in opposite directions under hydrostratic compression (V = instantaneous volume under compression, V_0 = initial volume). Reproduced with permission from ref[70]. © 2014 Macmillan Publishers Limited.

The double bundles (L2) contribute to lateral bonding, whereas the triple bundles (L3) contribute to inter-layer bonding. Therefore, each nanocluster involves 60 H-bonds in its solid state, i.e. 24 inter-nanocluster (lateral) and 36-inter-layer H-bonds. This anisotropic distribution of H-bonding number also allows preferential growth in the lateral direction. The experimental results combined with theoretical modelling have shown that under hydrostatic compression the superlattice displays pressure softening and undergoes solid-solid transition to a soft solid with bulk modulus of 16.7 GPa (Figure 3e).[70] Such a transition involves ligand flexure, which causes gear-like correlated chiral rotation of the nanoclusters. While the anisotropic ligand H-bonding is very fascinating, so far, no monolayer thick 2D structures have been reported. However, counter anion mediated control of crystal morphology has been shown (3D crystals).[71]

Next we deal an example where hydrogen bonding nanoclusters can direct self-assembly of other colloidal units. Previously, 1D nanocrystals and nanorods have been shown to produce mesoscopic aggregates upon (isotropic) electrostatic assembly, when mixed with oppositely charged plasmonic nanoparticles.[72] Importantly, the size dispersities have been shown to play a major role in determining the nature of superstructures. On the other hand, based on the crystal packing, the Ag_{44}-*p*MBA_{30} nanoclusters show anisotropic unique inter- and intralayer packing, which suggest their incorporation to promote novel specific assemblies. Specifically, it will be interesting to study how decorating a monodisperse 1D nano-objects with atomically precise Ag_{44}-*p*MBA_{30} will influence the higher order assembly through H-bonding. In this context, the Na_4-Ag_{44}-*p*MBA_{30} nanoclusters were explored to prepare a composite bilayer assembly of 1D tellurium nanowires (TeNWs, $l = 2.5$ µm, $d \sim 28$ nm) via air-water interface evaporation-induced assembly (**Figure 4**).[73] When pristine TeNWs were dispersed in 1-butanol and subsequently let to undergo air-water interface assembly, monolayer of TeNWs with parallel arrangement was observed. On the other hand, the TeNWs can be first surface modified with Na_4Ag_{44}-*p*MBA_{30} by mixing both the precursors (Na_4-Ag_{44}-*p*MBA_{30} and TeNWs) in *N,N*-dimethylformamide (DMF) followed by centrifugation.

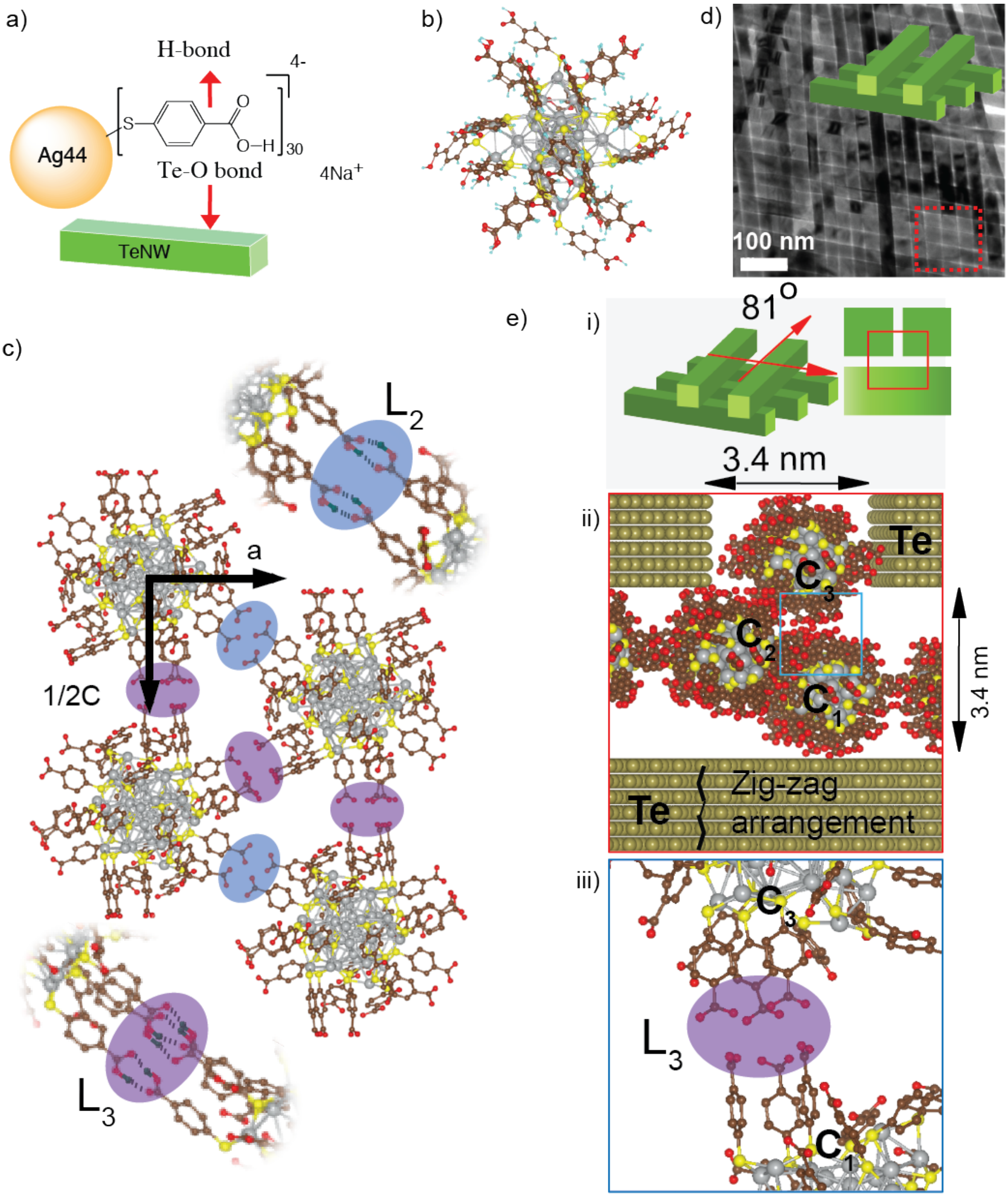

Figure 4. Composite tellurium nanowire (TeNW) bilayered structures directed by H-bondings between Na$_4$-Ag$_{44}$-*p*MBA$_{30}$ nanoclusters, denoted as Ag$_{44}$@TeNWs. a) Chemical structure and the underlying bondings. b) Structure of a Na$_4$-Ag$_{44}$-*p*MBA$_{30}$ nanocluster. c) Inter-nanoparticle H-bonding in Ag$_{44}$-*p*MBA$_{30}$ nanoclusters and Ag$_{44}$@TeNWs. d) TEM micrograph displaying crossed bilayer structure with an unusual angle of 81° between the TeNWs upon air-water interface assembly of Ag$_{44}$@TeNWs. e) Close-ups for the suggested packings of the

Ag_{44}@TeNWs bilayers, driven by the H-bonding between the Ag_{44}-*p*MBA_{30} nanoclusters. Reproduced with permission from ref[73]. 2016 WILEY-VCH Verlag GmbH & Co. KGaA, Weinheim.

The resulted Na_4-Ag_{44}-*p*MBA_{30} coated TeNWs are referred as Ag_{44}@TeNWs, mutually bound by Te-O interaction. Interestingly, when similar assembly process was applied for a dispersion of Ag_{44}@TeNWs, a crossed "woodpile-like" bilayer structure was observed instead of a monolayer, as illustrated by the TEM image in Figure 4d. The arrangement of TeNWs between the two layers in the composite bilayer showed an unusual angle of $\approx 81^o$ (Figure 4d,e). Based on concentration dependent experiments and modelling using the crystal structure of Ag_{44}-*p*MBA_{30},[70] it was shown that the different states of aggregation of Ag_{44}-*p*MBA_{30} are responsible for stabilizing the above woodpile-like structure. The arrangement of NWs between two layers at their mutual angle 81^o allow a strong hydrogen bonding due to three pairs (L3) of H-bonding between the Ag_{44}-*p*MBA_{30} coated over TeNWs (Figure 4c,e). However, selecting angles 90^o and 0^o would allow only either two or one pair of H-bonding, respectively. This strong interlayer H-bonding drives the unusual geometry and 2D layer formation. Therefore, there is a clear evidence that, unlike electrostatic interaction, atomically precise nanoclusters with directional H-bonding surface ligands can provide highly tunable nanostructures.

5. Self-assembled capsids

H-bonding stabilized spherical superstructures have previously been reported in the literature using 2-6 nm gold nanoparticles.[40] Using strictly monodisperse metal nanoclusters, the self-assembly of keplerates [Mo_{154}] was reported to spherical superstructures termed as "inorganic vesicle-like" structures (**Figure 5**).[74] There the self-assembly of macroanionic clusters was attributed to the H-bondings, directed by water molecules. Recent theoretical studies using Monte Carlo simulations have shown that the patchy distribution of interacting sites on the clusters is responsible for spherical structure.[5,6] On the other hand, reverse emulsion mediated assembly of spherical particles into colloidosomes have been shown to display plasmonic broadband absorption properties.[76]

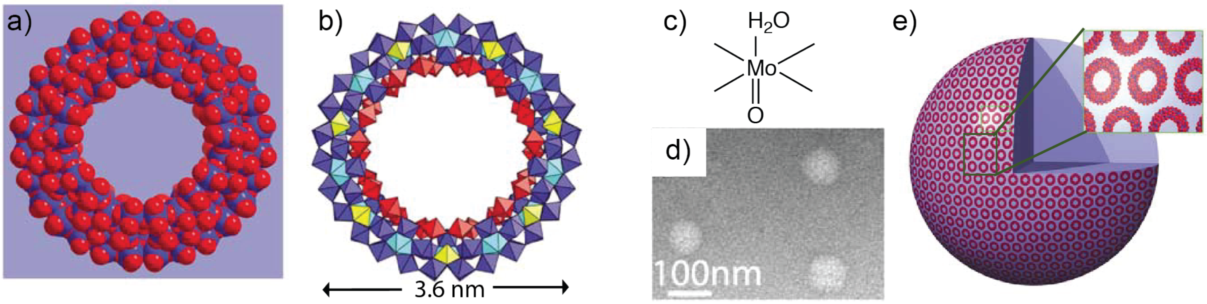

Figure 5. Inorganic vesicle-like particles derived from keplerates. a) X-ray structure in space-filling model of 3.6 nm [Mo_{154}] type nanowheel (Mo atoms in blue; O atoms in red). b) Polyhedral representation, showing pentagonal (Mo)Mo_5 units (in blue) (Mo_2 units in red, Mo_1 units in yellow). c) The smallest constituent units with a metal atom and ist coordination sphere, i.e., with one of the 70 H_2O ligands. d) TEM micrograph of self-assembled 45 nm vesicle-like particles. e) Schematic representation of the vesicle structure. Reproduced with permission from ref[74]. © 2003 Macmillan Publishers Limited.

Closed shell capsid-like assemblies can be obtained also by controlling the processing conditions. In Figure 2 we showed that atomically precise Au_{102}-*p*MBA_{44} (partly protonated ligands and partly in Na-salt form) spontaneosly self-assemble into monolayer 2D sheets, by dialysing from water to methanol. The slow dialysis process provides sufficient time for the nanoclusters to assemble in the hexagonal closed packing structure which maximizes the hydrogen bondings. By contrast, if an aqueous dispersion of partially deprotonated Au_{102}-*p*MBA_{44} nanoclusters is rapidly injected into methanol, spherical superstructures of average diameter of 200 nm are formed (**Figure 6**).[68] More importantly, the electron tomographic reconstruction showed that the spherical superstructures are hollow, involving a shell of a monolayer thickness (Figure 6b-d).

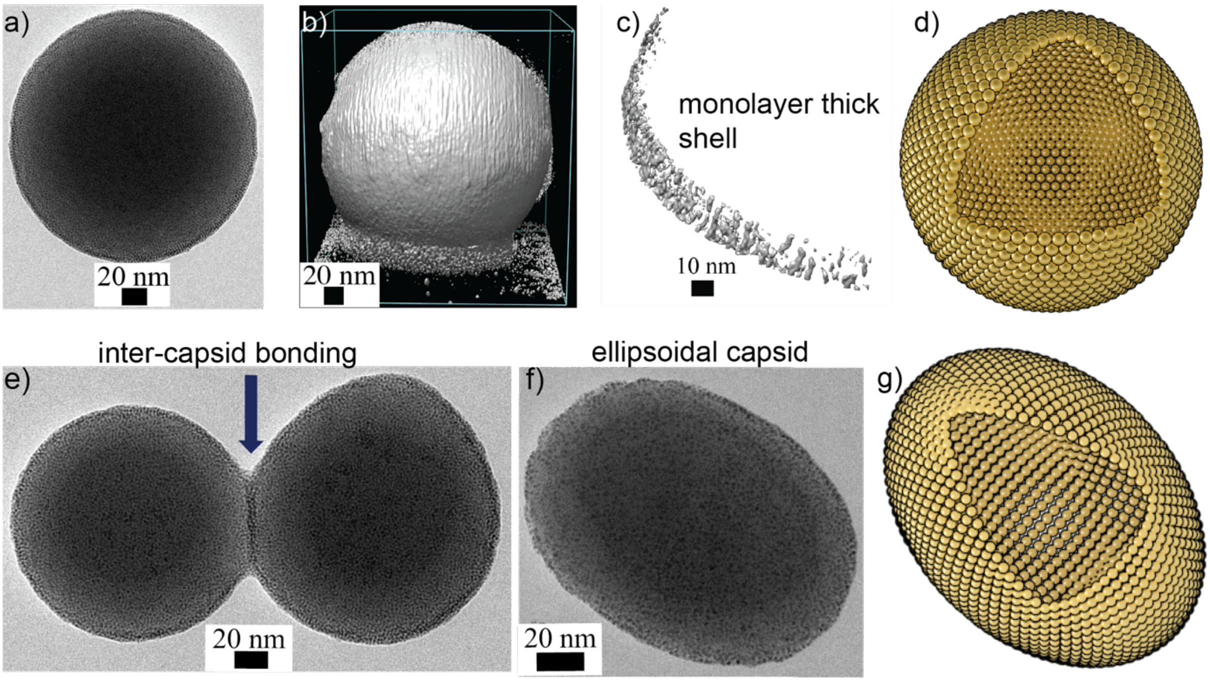

Figure 6. Colloidal capsids based on water dispersed Au$_{102}$-pMBA$_{44}$ (with a fraction of the total 44 *p*MBA ligands in the salt form) upon quickly injecting to large excess of methanol. a) TEM micrograph of self-assembled spherical capsid. b) An electron tomogram of a spherical capsid. c) A close-up of the tomogram showing a monolayer thick shell. d) Schematic illustration of a monolayer thick shell capsid. e) The capsids undergo supracolloidal assembly via inter-capsid H-bondings mediated by an ensemble of nanoclusters. f) TEM micrograph of an ellipsoidal capsid. g) Schematic illustration of an ellipsoidal capsid. Reproduced with permission from ref[68]. © 2016 WILEY-VCH Verlag GmbH & Co. KGaA, Weinheim.

Since the spherical structures are formed based on shape-defined atomically precise subunits and they are not amphiphilic, unlike conventional surfactants (which form vesicles), we termed the hollow spherical structures as “colloidal capsids”. The curvature of the shell is, in fact, expected as the rapid injection promotes packing defects, as has been proposed for many spherical superstructures.[5,6] The spherical structures, internally stabilized by H-bonds, are of particular interest as they allow reversible assembly. Beyond that, inter-capsid H-bonding allows also higher order structures and even hollow lightweight materials upon consequent packings, as will be discussed later. The inter-capsid H-bonding is directly illustrated by fusion of two capsids (Figure 6e). Further, our studies have shown that in addition to spherical capsids, ellipsoidal capsids such as the one shown in Figure 6g were also observed. 3D reconstruction using electron tomography (See Supporting Information, **Figure S1**, **Videos S1 and S2**) revealed that the capsids are stable upon drying and further showed that the shell is of monolayer thickness. We foresee that the ellipsoidal capsids can be formed either due to the fusion of two capsids or rearrangement of defects upon assembly.[5,6] However, at this point the mechanisms of formation and details how to tune the ellipsoidal capsid shells are not yet known.

6. Magnetic colloidal capsids and hydrogen bonded higher level superstructures

The above examples show self-assemblies based on exactly defined nanoclusters, where the number of the metal atoms (core) and the number of the ligands (surface) are exactly defined. Further, the gold nanocluster-based capsid illustrates the possibilities to fine tune the interactions between the capsids to realize higher order structures. However, the synthesis of such nanoclusters involves extensive purification steps. Therefore, it is relevant to ask whether simpler and more scalable single-step syntheses could be identified, allowing still some of the above observations, such as the colloidal capsids. Further, it could be relevant to ask if external fields/conditions can drive higher order capsids structures. Therein magnetic field was expected to be particularly attractive.

As an attempt to address this, we reported a rapid, in-situ, template-free single-step self-assembly of cobalt nanoparticles and their reversible superparamagnetic colloidal capsids using molecular precursors.[76] In this method, the knowledge gained from the self-assembly of atomically precise gold nanoclusters was implemented for the ligand engineering, i.e. that the ligand ditopic architecture around the metal core was expected to involve patchiness and broken symmetry. That this could be possible, was suggested by modelling a cobalt (Co) cluster using a ditopic ligand *p*-aminobenozic acid (*p*ABA) (Figure 1d) having an amino end which binds to the Co-metal, carboxylic acid end, facilitating hydrogen bonds, and the phenyl spacer. The model cluster Co_{13}-*p*ABA_{12} indeed suggested the anticipated ligand orientation towards the equator, like in the gold nanoclusters (Figure 2e,f). Encouraged by this, experiments were undertaken, aiming at particularly simple single-step synthesis.[76] The approach was in part inspired by the so-called heating-up synthesis, which was previously used to prepare surfactant-protected Cobalt nanoparticles.[77] By contrast, in the present case the capsids were prepared by mixing dicobalt octacarbonyl, $Co_2(CO)_8$ and a ditopic supramolecular interaction facilitating ligand *p*ABA (instead of the previously used surfactant-like ligands) in 1.0: 0.4 mol ratio in 1,2-dichlorobenzene at room temperature, followed by heating at 165 ^{o}C for 20 minutes, followed by cooling. This allowed superparamagnetic cobalt nanoparticles decorated with *p*ABA units (Co-*p*ABA) with narrow size distribution (*d*~5 nm), **Figure 7**. Upon cooling to the room temperature, the Co-*p*ABA nanoparticles spontaneously assembled into spherical capsids. This is attributed to the carboxylic acid dimerization driven nanoparticle assembly due to the apolar nature of the 1,2-DCB solvent (dielectric constant 9.93). Based on time resolved TEM, it was shown that the nanoparticle (Figure 7a) formation occurs within five minutes after starting of the reaction. The 3D structural details using electron tomographic reconstruction revealed that the capsids are made up of a few layer thick (~25 nm) shells (Figure 7b, c). Interestingly, the TEM micrographs displayed capsids with varying contrast differences between the shells and the interior. This is due to the excess *p*ABA molecules that are not bound to nanoparticle surface, which are statistically trapped inside the capsids (Figure 7e,f). Furthermore, the nanoparticles do not show well ordered arrays within the shell due to their non-uniform size dispersities (Figure 7d).

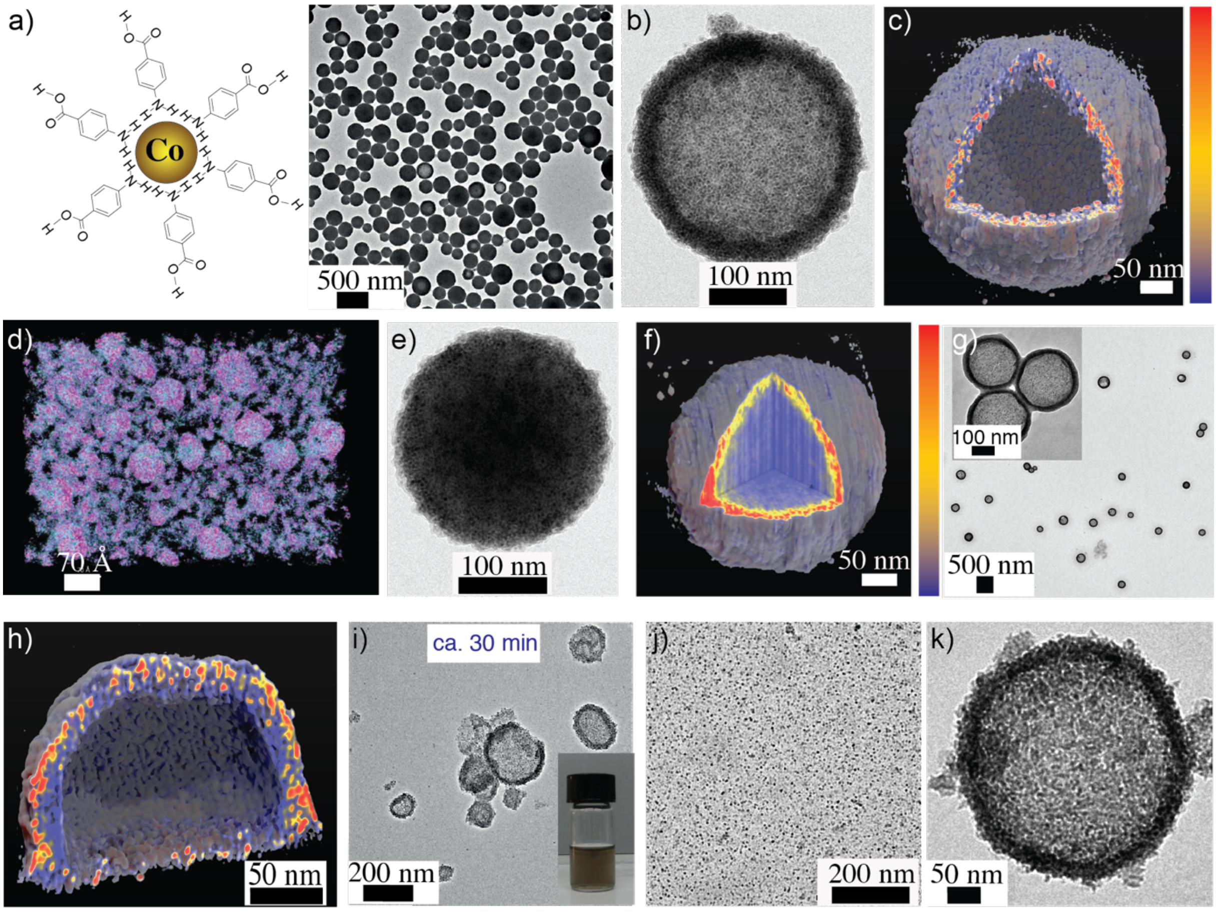

Figure 7. Heating-up synthesis of Co-*p*ABA nanoparticles (CoNP) in 1,2-DCB and the subsequent in-situ template-free self-assembly to capsids upon cooling. a) Schematic representation of ditopic ligand protected CoNPs and low magnification TEM micrograph of an ensemble of colloidal capsids. b) TEM of a single hollow capsid. c) Electron tomogram (ET) reconstruction showing 3D structure of a hollow capsid with the shell consisting a few layers of Co-*p*ABA. d) A close-up from the shell illustrating that the nanoparticles do not show well-defined packing order. e) After the synthesis, a fraction of the *p*ABA ligands can remain unbound from the cobalt surface, and they can be trapped in the capsid, as shown in a TEM micrograph by the reduced contrast between the core and shell, in comparison to b). f) ET reconstruction showing shell and trapped ligands in the capsid interior. g) Upon exchanging the solvent from 1,2-DCB to acetone allows to remove the potentially trapped unreacted ligands from the capsid interior, as revealed by TEM and ET reconstruction, thus allowing the purified capsids (h). i-k) shows capsid disassembly and reassembly upon exchanging 1,2-DCB to

methanol and redispersion in 1,2-DCB. Reproduced with permission from ref.[76] © 2017 WILEY-VCH Verlag GmbH & Co. KGaA, Weinheim.

The presence of inter-nanoparticle H-bonding was supported using solvent exchange from 1,2-DCB to methanol and acetone. When solvent was exchanged to acetone (dielectric constant 20.7), only the trapped *p*ABA molecules were released from the interior leaving the purified capsids with deformed shell upon drying (Figure 7g, h). In methanol (dielectric constant 32.7), the capsids were disrupted into individual Co-*p*ABA nanoparticles (Figure 7i, j). These individual nanoparticles obtained after dispersing in methanol, again rendered hollow capsids upon adding 1,2-DCB (Figure 7k). The re-assembled capsids displayed similar dimensions and shell thickness as that of the freshly synthesized capsids, suggesting that the capsid formation is a template-free reversible assembly. In addition, the capsids were shown to undergo thermoreversible assembly, further supporting the H-bonding mediated self-assembly.

The capsids were superparamagnetic due to the small size of individual nanoparticles (the magnetic core of 3.2 nm and average overall size ~ 5 nm). This property was exploited to achieve higher order 1D-capsid chains of several micrometers, based on driving of the capsids into chains, whereupon the H-bonds were established between the neighbouring capsids (**Figure 8a-c**). In this way directional H-bonds were activated by imposing by magnetic fields. Curiously, due to strong H-bonding, the capsid-chains were stable upon removing the magnetic fields, and even for selected solvent exchanges, thus providing an opportunity to construct light-weight mesoscale polymeric chains with the capsids as repeat units. Further, macroscopic films composed of hollow capsids were demonstrated using air-water interface assembly by dispersing the capsids in tolune followed by placing the dispersion on water in a petri-dish. This furnished a highly light weight porous colloidal framework material (Figure 8d-g).

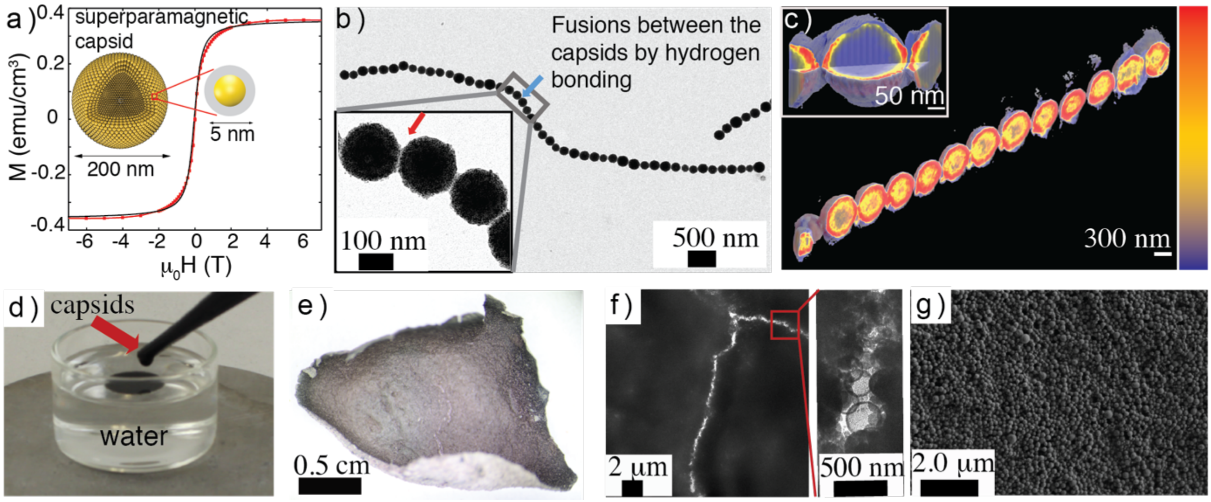

Figure 8. Higher level structures of Co-*p*ABA capsids. a) The magnetic hysteresis curve for Co-*p*ABA capsids indicating superparamagnetic properties. b) Magnetic field drives capsids to chains, subsequently stabilized by intercapsid H-bonding even removing the magnetic field. c) ET reconstruction of a capsid chain. a) Air-water self-assembly of capsids to films. e) A bulk porous film composed of capsids. f) Hollow capsids shown by TEM micrographs of film. g) SEM image showing surface of bulk film. Reproduced with permission from ref[76]. © 2017 WILEY-VCH Verlag GmbH & Co. KGaA, Weinheim.

In the capsid formation the ligand structure and the position of functional groups (-NH_2 and -COOH) was found to play an important role. Among the ligands studied, only the *para*-coupled *p*ABA showed capsid formation, eg., when compared with *ortho*- and *meta*-coupled molecules *o*ABA or *m*ABA. In the latter ones, the H-bonds between the ligands of the neighbouring nanoparticles would be suppressed due to steric effects. The formation of multilayered shells is attributed to the polydispersed nature of building blocks. The rapid aggregation of the nanoparticles in apolar 1,2-DCB solvent is expected due to low dielectic constant. By contrast to aq. gold nanoclusters, where a balance between attraction and repulsive forces were achieved to obtain ordered structures with ligands partly in the salt form, the cobalt nanoparticles experience solely strong H-bonding dimerization.

In the following section we will describe our new findings on the effect of ligand structure on capsid morphology. For this, 6-amino-2-naphthoic (denoted as *p*ANA, **Figure 1c**) acid was chosen, since the position and orientation of amino and carboxylic acid groups resemble that of *p*ABA.

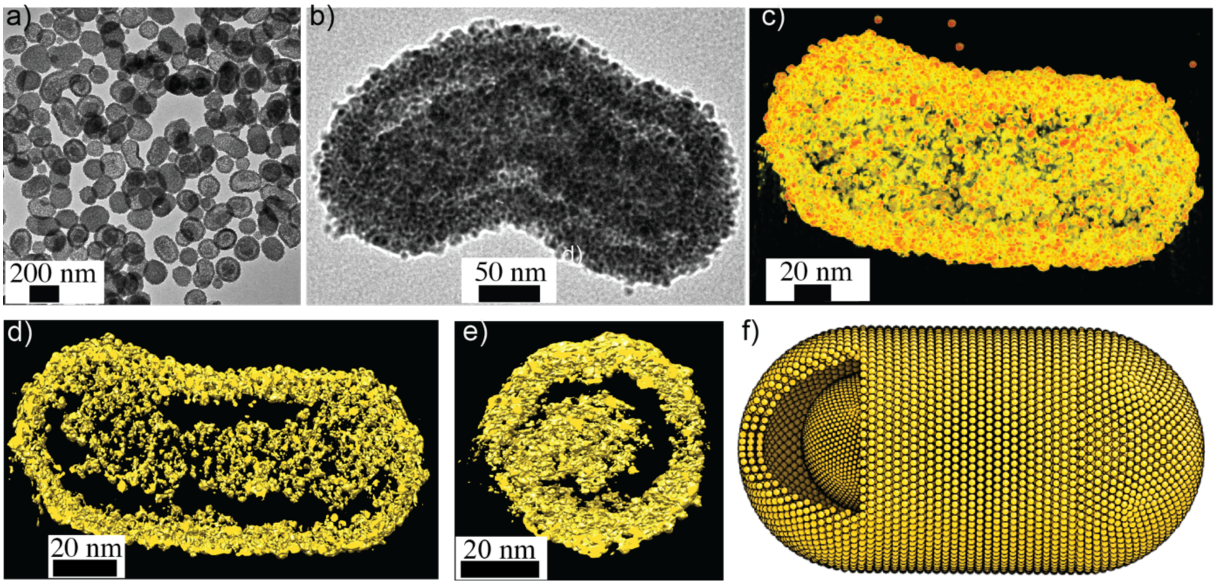

Figure 9. Cylindrical capsids based on Co-*p*ANA. a) Low magnification TEM micrograph. b) TEM of a cylindrical capsid, also showing another rod-like assembly in the interior. c) 3D structure of capsid resolved using ET reconstructions. d and e) The lateral and vertical views of the capsid showing 20 nm thick shell and the interior rod-like assembly, 50 nm in diameter. e) Schematic representation of a cylindrical capsid encapsulating rod-like assembly.

The synthesis was performed similarly as that of Co-*p*ABA reported earlier (see Supporting Information for details).[76] Interestingly, the TEM micrographs of the samples prepared from the reaction mixture revelead predominantly cylindrical capsids (**Figure 9**). Curiously, the capsids contain rod-like nanoparticle assembly (*d*~50 nm) in the interior (Figure 9b). A systematic analysis using ET revelead that the capsids are composed of shells consisting a few layers of nanoparticles (~20 nm thick) with an average length of 200 nm and diameter of 100 nm (Supporting Information, **Figure S2**, **Video S3**). The sizes of the individual building blocks were similar to those of Co-*p*ABA nanoparticles. The determination of magnetic properties revealed the superparamagnetic behavior of the capsids (Figure S3). This suggests that by careful ligand engineering the structure of the capsids can be tuned towards novel assemblies.

7. Conclusions.

Colloidal self-assembly is a strongly growing area of research, where nanoparticle self-assembly is one of the key areas. Like supramolecular chemistry has matured to offer a rich toolbox to construct functional structures beyond the individual molecular scale, a challenge would be to develop rational methods for supracolloidal chemistry, i.e. structures beyond the colloidal scale using colloidal level building blocks. Various self-assembled superstructures have already been shown mostly based on nanoparticles with various widths of their size distributions and stabilizations by surfactant-like ligands. Still, one could expect that unforeseen self-assemblies and related functions could be possible upon better control of the polydispersity until atomic precision and using more functional ligands, beyond surfactants. In this feature article we have provided a glimpse for the future new possibilities using some elementary structures. We show that by providing exactly defined metal cores with exactly defined number of ligands, also mediating supramolecular interactions between the nanoparticles, spontaneous template-free self-assembly to 2D colloidal materials becomes possible if a "gentle" and slow processing is selected to allow sufficient time to suppress defects. This follows from the slightly surprising observation that the ligand architecture around the nanoparticles is not necessarily isotropic but can involve a broken symmetry from isotropic arrangement to directional "patches" to increase the supramolecular interactions in 2D. To exploit such properties in more generally, much deeper understanding has to be developed to understand and control the ligand structures on nanoparticles. One can next relieve conditions from the nanoparticle atomic precision and slow processing. If slow processing is relieved, defects are more prone, thus leading to curvature and further to closed shells, i.e. capsids. On the other hand, relieving the condition of exactly defined size until narrow polydispersity, capsids with H-bonding ligands are similarly formed due to inherent packing problems. Higher order structures can be achieved by imposing external fields, which can direct arrangements of the capsids, whereupon hydrogen bonds between the capsids become activated in the directions of the nanoparticle close contacts, thus stabilizing the higher order structures even by removing the external fields. Finally, we provide an example, how the anisotropic colloidal interactions of H-bonding nanoparticles can direct colloidal self-assemblies of eg. nanorods. The examples discussed in this article include 2D nanosheets, composite bilayers, spherical-, ellipsoidal-, and rod-like capsids with potential application as porous colloidal framework materials. Further, nanoclusters possess unique and tunable optical properties (e.g. luminescence), catalytic activities and low in-vivo toxicity compared to large plasmonic nanoparticles.[78] Therefore, we foresee that combining these properties with 2D self-assembly or capsid shells will pave way for new sensors for imaging, selective carriers or nanoconfinement delivery vehicles. Further, in materials science point of view, the 2D assemblies can be utilized in combination with other 2D nanosheets such as metal chalcogenides to enhance the electrocataltyic activity.[79] Such hybrid materials hold promise for hydrogen generation via water splitting for future energy storage applications. We strongly believe that the knowledge obtained from such studies will advance the rational design of colloidal assemblies in general towards new generation of supracolloidal functional materials.

Supporting Information

Supporting Information is available from the Wiley Online Library or from the authors.

Acknowledgements

We acknowledge Academy of Finland Centre of Excellence in Molecular Engineering of Biosynthetic Hybrid Materials (HYBER), and ERC Advanced Grant (ERC-2011-AdG-291364-MIMEFUN) are acknowledged. This work made use of the CSC-IT centre (Espoo) computational facilities and Aalto University Nanomicroscopy Center (Aalto-NMC) premises. We acknowledge Dr. A. Som and Prof. T. Pradeep for the providing the coloured originals for Figure 4 panels.

Received: ((will be filled in by the editorial staff))
Revised: ((will be filled in by the editorial staff))
Published online: ((will be filled in by the editorial staff))

References

[1] C. Schliehe, B. H. Juarez, M. Pelletier, S. Jander, D. Greshnykh, M. Nagel, A. Meyer, S. Foerster, A. Kornowski, C. Klinke, H. Weller, *Science* **2010**, *329*, 550-553.

[2] C. Tan, X. Cao, X.-J. Wu, Q. He, J. Yang, X. Zhang, J. Chen, W. Zhao, S. Han, G.-H. Nam, M. Sindoro, H. Zhang, *Chem. Rev.* **2017**, *117*, 6225−6331.

[3] M. Nasilowski, B. Mahler, E. Lhuillier, S. Ithurria, B. Dubertret, *Chem. Rev.* **2016**, *116*, 10934–10982.

[4] C. Tan, H. Zhang, *Nat. Commun.* **2015**, *6*, 7873.

[5] E. Mani, E. Sanz, S. Roy, M. Dijkstra, J. Groenewold, W. K. Kegel, *J. Chem. Phys.* **2012**, *136*, 144706.

[6] D. S. Roshal, K. Y. Petrov, A. E. Myasnikova, S. B. Rochal, *Phys. Lett. A* **2014**, *378*, 1548–1552.

[7] Y. Han, Y. Shokef, A. M. Alsayed, P. Yunker, T. C. Lubensky, A. G. Yodh, *Nature* **2008**, *456*, 898-903.

[8] D. J. Kushner, *Bacteriol. Rev.* **1969**, *33*, 302–345.

[9] W. H. Roos, R. Bruinsma, G. J. L. Wuite, *Nat. Phys.* **2010**, *6*, 733–743.

[10] F.H. C. Crick, J. D. Watson, *Nature* **1956**, *177*, 473–475.

[11] D. L. D. Caspar, *Adv. Protein Chem.* **1963**, *18*, 37–121.

[12] A. Hernandez-Garcia, D. J. Kraft, A. F. J. Janssen, P. H. H. Bomans, N. A. J. M. Sommerdijk, D. M. E. Thies-Weesie, M. E. Favretto, R. Brock, F. A. de Wolf, M. W. T. Werten, P. van der Schoot, M. C. Stuart, R. de Vries, *Nat. Nanotechnol.* **2014**, *9*, 698-702.

[13] A. J. Olson, Y. H. E. Hu, E. Keinan, *Proc. Nat. Acad. Sci.* **2007**, *104*, 20731–20736.

[14] Y. Li, Y. Lai, X. Xu, X. Zhang, Y. Wu, C. Hu, Z. Gu, *Nanomed. Nanotech. Biol. Med.* **2016**, *12*, 355-364.

[15] J. Xu, J. Li, Y. Yang, K. Wang, N. Xu, J. Li, R. Liang, L. Shen, X. Xie, J. Tao, J. Zhu, *Angew. Chem. Int. Ed.* **2016**, *55*,14633 –14637.

[16] V. N. Manoharan, *Science* **2015**, *349*, 1253751

[17] a) Z. Quan, J. Fang, *Nano Today* **2010**, *5*, 390-411. b) K. Miszta, J. de Graaf, G. Bertoni, D. Dorfs, R. Brescia, S. Marras, L. Ceseracciu, R. Cingolani, R. van Roij, M. Dijkstra, L. Manna, *Nat. Mater.* **2011**, *10*, 872–876.

[18] B. Derjaguin, *Acta Phys. Chim. U.S.S.R.* **1939**, *10*, 333-346.

[19] B. Derjaguin, L. D. Landau, *Acta Phys. Chim. U.S.S.R.* **1941**, *14*, 633-662.

[20] E. J. W. Verwey, J. T. G. Overbeek, *Theory of Stability of Lyophobic Colloids*. Elsevier, Amsterdam, the Netherlands **1948**.

[21] Y. Liang, N. Hilal, P. Langston, V. Starov. *Adv. Colloid Interface Sci.* **2007**, *134-135*, 151-166. b) B. W. Ninham. *Adv. Colloid Interface Sci.* **1999**, *83*, 1-17.

[22] Y. S. Lee, *Self-assembly and nanotechnology: a force balance approach*. **2008**, John Wiley & Sons, Inc., Hoboken, USA 2008.

[23] Q. Chen, J. Yan, J. Zhang, S. C. Bae, S. Granick, *Langmuir* **2012**, *28*, 13555–13561

[24] a) Y. Wang, Y. Wang, D. R. Breed, V. N. Manoharan, L. Feng, A. D. Hollingsworth, M. Weck, D. J. Pine, *Nature* **2013**, *491*, 51–55. b) Y. Wang, O. Zeiri, A. Neyman, F. Stellacci, I. A. Weinstock, *ACS Nano* **2012**, *6*, 629-640. c) R. Huang, R. P. Carney, F. Stellacci, B. L. T. Lau, *Langmuir* **2013**, *29*, 11560−11566.

[25] S. Sacanna, D. J. Pine, G.–R. Yi, *Soft Matter* 2**013**, *9*, 8096-8106. b) F. Li, D. P. Josephson, A. Stein, *Angew. Chem. Int. Ed.* **2011**, *50*, 360–388.

[26] P. L. Biancaniello, A. J. Kim, J. C. Crocker, *Phys. Rev. Lett.* **2005**, *94*, 058302.

[27] a) A. H. Gröschel, A. Walther, T. I. Löbling, F. H. Schacher, H. Schmalz, A. H. E. Müller, *Nature* **2013**, *503*, 247–251. b) T. I. Löbling, O. Borisov, J. S. Haataja, O. Ikkala, A. H. Gröschel, A. H. E. Müller, *Nat. Commun*. **2016**, *7*, 12097.

[28] a) C. A. Mirkin, R. L. Letsinger, R. C. Mucic, J. J. Strohoff, *Nature* **1996**, *382*, 607-609. b) A. P. Alivisatos, K. P. Johnsson, X. Peng, T. E. Wilson, C. J. Loweth, M. P. Bruchez Jr, P. G. Schultz, *Nature* **1996**, *382*, 609-611.

[29] a) C. R. van den Brom, P. Rudolf, T. T. M. Palstra, B. Hessen, *Chem. Commun*. **2007**, 4922-4924. b) C. R. van den Brom, I. Arfaoui, T. Cren, B. Hessen, T. T. M. Palstra, J. T. M. De Hosson, P. Rudolf, *Adv. Funct. Mater.* **2007,** *17*, 2045–2052.

[30] G. Schmid, R. Pfeil, R. Boese, F. Bandermann, S. Meyer, G. H. M. Calis, J. W. A. van der Velden, *Eur. J. Inorg. Chem*. **1981**, *114*, 3634–3642.

[31] W. W. Weare, S. M. Reed, M. G. Warner, J. E. Hutchison, *J. Am. Chem. Soc*. **2000**, *122*, 12890–12891.

[32] M. Brust, M. Walker, D. Bethell, D. J. Schiffrin, R. Whyman, *J. Chem. Soc. Chem. Commun*. **1994**, 801-802.

[33] M. J. Hostetler, S. J. Green, J. J. Stokes, R. W. Murray, *J. Am. Chem. Soc*. **1996**, *118*, 4212-4213.

[34] a) *Nanoparticle assemblies and superstructures,* (Ed: N. A. Kotov), CRC Press, Taylor and Francis Group, Boca Raton, USA **2006**. b) A. Verma, O. Uzun, Y. Hu, Y. Hu, H.-

S. Han, N. Watson, S. Chen, D. J. Irvine, F. Stellacci, *Nat. Mater* **2008***, 7*, 588-595. c) C. M. Jewell, J.-M. Jung, P. U. Atukorale, R. P. Carney, F. Stellacci, D. J. Irvine, *Angew. Chem. Int. Ed.* **2011***, 50*, 12312 –12315

[35] D. Luo, C. Yan, T. Wang, *Small* **2015**, *11*, 5984–6008.

[36] A. M. Kalsin, M. Fialkowski, M. Paszewski, S. K. Smoukov, K. J. M. Bishop, B. A. Grzybowski, *Science* **2006**, *312*, 420-424.

[37] M. E. Leunissen, C. G. Christova, A.-P. Hynninen, C. P. Royall, A. I. Campbell, A. Imhof, M. Dijkstra, R. van Roij, A. van Blaaderen, *Nature* **2005**, *437*, 235-240.

[38] E. V. Shevchenko, D. V. Talapin, N. A. Kotov, S. O'Brien, C. B. Murray. *Nature* **2006**, *439*, 55-59.

[39] M. A. Kostiainen, P. Hiekkataipale, A. Laiho, V. Lemieux, J. Seitsonen, J. Ruokolainen, P. Ceci, *Nat. Nanotechnol.* **2013**, *8*, 52–56.

[40] Y. Xia, T. D. Nguyen, M. Yang, B. Lee, A. Santos, P. Podsiadlo, Z. Tang, S. C. Glotzer, N. A. Kotov, *Nat. Nanotech.* **2011**, *6*, 580–587.

[41] a) A. K. Boal, F. Ilhan, J. E. DeRouchey, T. Thurn-Albrecht, T. P. Russell, V. M. Rotello, *Nature* **2000**, *404*, 746-748. b) M. M. A. Kashem, D. Patra, J. Perlich, A. Rothkirch, A. Buffet, S. V. Roth, V. M. Rotello, P. Müller-Buschbaum, *ACS Macro Lett.* **2012**, *1*, 396–399.

[42] a) L. Han, J. Luo, N. N. Kariuki, M. M. Maye, V. W. Jones, C. J. Zhong, *Chem. Mater.* **2003**, *15*, 29–37. b) W. Zheng, M. M. Maye, F. L. Leibowitz, C.–J. Zhong, *Anal. Chem.* **2000**, *72*, 2190–2199.

[43] E. Hao, T. Lian, *Chem. Mater*. **2000**, *12*, 3392–3396.

[44] W. B. Rogers, V. N. Manoharan, *Science* **2015**, *347*, 639-642.

[45] R. Baron, C.-H. Huang, D. M. Bassani, A. Onopriyenko, M. Zayats, I. Willner, *Angew. Chem. Int. Ed.* **2005**, *44,* 4010–4015.

[46] M. N. O´Brien, H.-X. Lin, M. Girard, M. Olvera de la Cruz, C. A. Mirkin, *J. Am. Chem. Soc.* **2016**, ***138***, 14562–14565.

[47] P. D. Jadzinsky, G. Calero, C. J. Ackerson, D. A. Bushnell, R. D. Kornberg, *Science* **2007**, *318*, 430–433. b) Y. Levi-Kalisman, P. D. Jadzinsky, N. Kalisman, H. Tsunoyama, T. Tsukuda, D. A. Bushnell, R. D. Kornberg, *J. Am. Chem. Soc.* **2011**, *133*, 2976–2982.

[48] a) I. Chakraborty, T. Pradeep, *Chem. Rev.* **2017**, *117*, 8208−8271. b) H. Qian, M. Zhu, Z. Wu, R. Jin, *Acc. Chem. Res.* **2012**, *45*, 1470–1479.

[49] a) R. Jin, *Nanoscale* **2015**, *7*, 1549–1565. b) R. Jin, C. Zeng, M. Zhou, Y. Chen, *Chem. Rev.* **2016**, *116*, 10346–10413.

[50] C. Zeng, Y. Chen, K. Kirschbaum, K. J. Lambright, R. Jin, *Science* **2016**, *354*, 1580-1584.

[51] a) M. Azubel, J. Koivisto, S. Malola, D. Bushnell, G. L. Hura, A. L. Koh, H. Tsunoyama, T. Tsukuda, M. Pettersson, H. Häkkinen, R. D. Kornberg, *Science* **2014**, *345*, 909–912. b) K. Salorinne, S. Malola, O. A. Wong, C. D. Rithner, X. Chen, C. J. Ackerson, H. Häkkinen, *Nat. Commun*. **2016**, *7*, 10401.

[52] H. Häkkinen, *Nat. Chem.* **2012**, *4*, 443–455

[53] N. A. Kotov, *Science* **2010**, *330*, 188-189.

[54] C. Yi, H. Zheng, L. M. Tvedte, C. J. Ackerson, K. L. Knappenberger, *J. Phys. Chem.* C. **2015**, *119*, 6307–6313.

[55] K. S. Novoselov, A. K. Geim, S. V. Morozov, D. Jiang, Y. Zhang, S. V. Dubonos, I. V. Grigorieva, A. A. Firsov, *Science* **2004**, *306*, 666-669.

[56] K. S. Novoselov, A. K. Geim, S. V. Morozov, D. Jiang, M. I. Katsnelson, I. V. Grigorieva, S. V. Dubonos, A. A. Firsov, *Nature* **2005**, *438*, 197-200.

[57] C. Weisbuch, B. Vinter, *Quantum semiconductor structures: fundamentals and applications*. Academic Press, Inc., San Diego, USA, **1991.**

[58] X. Li, G. Zhang, X. Bai, X. Sun, X. Wang, E. Wang H. Dai. *Nat. Nanotech.* **2008**, *3*, 538-542.

[59] R. Jin, Y. C. Cao, E. Hao, G. S. Métraux, G. C. Schatz, C. A. Mirkin, *Nature* **2003**, *425*, 487-490.

[60] a) R. Geick, C. H. Perry, G. Rupprecht, *Phys. Rev*. **1966**, *146*, 543-547. b) T. Sekine, H. Kanda, Y. Bando, M. Yokoyama, K. A. Hojou, *J. Mater. Sci. Lett*. **1990**, *9*, 1376−1378. c) M. Naguib, V. N. Mochalin, M. W. Barsoum, Y. Gogotsi, Y. *Adv. Mater*. **2014**, *26*, 992−1005. d) Y. Omomo, T. Sasaki, L. Wang, M. Watanabe, *J. Am. Chem. Soc.* **2003**, *125*, 3568−3575.

[61] M. Zhao, Y. Wang, Q. Ma, Y. Huang, X. Zhang, J. Ping, Z. Zhang, Q. Lu, Y. Yu, H. Xu, Y. Zhao, H. Zhang, *Adv. Mater*. **2015**, *27*, 7372–7378. b) R. Sakamoto, K. Takada, T. Pal, H. Maeda, T. Kambe, H. Nishihara, *Chem. Commun*. **2017**, *53*, 5781-5801.

[62] T. Yu, B. Lim, Y. Xia, *Angew. Chem. Int. Ed*. **2010**, *49*, 4484–4487.

[63] Y. Liu, Z. Wu, H. Zhang, *Adv. Colloid Interface Sci*. **2014**, *207*, 347–360.

[64] Y. Suzuki, G. Cardone, D. Restrepo, P. D. Zavattieri, T. S. Baker, F. A. Tezcan, *Nature* **2016**, *533*, 369–373.

[65] P. Kissel, D. J. Murray, W. J. Wulftange, V. J. Catalano, B. T. King, *Nat. Chem.* **2014**, *6*, 774-778.

[66] M. J. Kory, M. Wörle, T. Weber, P. Payamyar, S. W. van de Poll, J. Dshemuchadse, N. Trapp, A. D. Schlüter, *Nat. Chem*. **2014**, *6*, 779-784.

[67] M. Chhowalla, H. S. Shin, G. Eda, L.-J. Li, K. P. Loh, H. Zhang, *Nat. Chem*. **2013**, *5*, 263–275.

[68] Nonappa, T. Lahtinen, J. S. Haataja, T.-R. Tero, H. Häkkinen, O. Ikkala, *Angew. Chem. Int. Ed*. **2016**, 55, 16035–16038.

[69] A. Desireddy, B. E. Conn, J. Guo, B. Yoon, R. N. Barnett, B. M. Monahan, K. Kirschbaum, W. P. Griffith, R. L. Whetten, U. Landman, T. P. Bigioni, *Nature* **2013**, *501*, 399–402.

[70] B. Yoon, W. D. Luedtke, R. N. Barnett, J. Gao, A. Desireddy, B. E. Conn, T. Bigioni, U. Landman, *Nat. Mater.* **2014**, *13*, 807–811.

[71] Q. Yao, Y. Yu, X. Yuan, Y. Yu, D. Zhao, J. Xie, J. Y. Lee, *Angew. Chem. Int. Ed.* **2014**, *54*, 184–189.

[72] a) J. Majoinen, J. Hassinen, J. S. Haataja, H. T. Rekola, E. Kontturi, M. A. Kostiainen, R. H. A. Ras, P. Törmä, O. Ikkala, *Adv. Mater.* **2016**, *28*, 5262–5267. b) V. Liljeström, A. Ora, J. Hassinen, H. Rekola, Nonappa, M. Heilala, J. Joensuu, R. H. A. Ras, P. Törmä, O. Ikkala, M. A. Kostiainen, *Nat. Commun.* **2017**, accepted

[73] A. Som, I. Chakraborty, T. A. Maark, S. Bhat, T. Pradeep, *Adv. Mater*. **2016**, *28*, 2827–2833.

[74] T. Liu, E. Diemann, H. Li, A. W. M. Dress, A. Müller, *Nature* **2003**, *426*, 59-62

[75] D. Liu, F. Zhou, C. Li, T. Zhang, H. Zhang, W. Cai, Y. Li, *Angew. Chem. Int. Ed.* **2015**, *54,* 9596 –9600.

[76] Nonappa, J. S. Haataja, J. V. I. Timonen, S. Malola, P. Engelhardt, N. Houbenov, M. Lahtinen, H. Häkkinen, O. Ikkala, *Angew. Chem. Int. Ed*. **2017**, 56, 6473-6477.

[77] a) V. F. Puntes, K. M. Krishnan, A. P. Alivisatos, *Science* **2001***, 291*, 2115-2117. b) J. V. I. Timonen, E. T. Seppälä, O. Ikkala, R. H. A. Ras, *Angew. Chem. Int. Ed.* **2011***, 50*, 2080-2084.

[78] *Protected metal clusters from fundamentals to applications* In *Frontiers of Nanoscience* **2015**, *9*, 1-358. (Ed: T. Tsukuda, H. Häkkinen), Elsevier Publishers, Amsterdam, Netherlands.

[79] Z. Yin, B. Chen, M. Bosman, X. Cao, J. Chen, B. Zheng, H. Zhang, *Small* **2014**, *10*, 3537–3543.

Dr. Nonappa received PhD in 2008 under the guidance of Prof. Uday Maitra from IISc, Bangalore, India on the synthesis of rare bile acids and supramolecular gels. After postdoctoral research at the University of Jyväskylä, Finland, on soft matter solid state NMR with Prof. Erkki Kolehmainen, he joined the group of Prof. Olli Ikkala at the Department of Applied Physics, Aalto University, where he is now an Adjunct Professor (Docent) in soft matter microscopy and Research Fellow at the Department of Bioproducts and Biosystems. His current research interests are colloidal self-assembly and soft matter electron tomography.

Prof. Olli Ikkala heads Molecular Materials laboratory of Aalto University and Centre of Excellence of Academy of Finland. After PhD 1983 in materials physics at Helsinki University of Technology, he worked 10 years in chemical industry developing conducting polymers, thereafter returning to Helsinki University of Technology (now Aalto University). He has been awarded twice ERC Advanced Grant, twice Academy Professorship of Academy of Finland, and is elected in Finnish Academy of Science and Letters and Technology Academy of Finland. Presently he has part time visitor at Université Grandes Alpes, Grenoble. His interests cover functional materials by hierarchical self-assemblies and biomimetics.

The table of contents entry

Unforeseen colloidal self-assemblies and hierarchies and related functions are expected upon control of the polydispersity of nanoparticles until atomic precision and using functional ligands incorporating supramolecular motifs, beyond surfactants. We describe 2D colloidal crystal, composite bilayers, spherical-, ellipsoidal-, and rod-like capsids with potential application as porous supracolloidal materials.

Keyword: Nanoparticles, supracolloidal self-assembly, hydrogen bonding, capsids, 2D colloidal crystals

Authors: Nonappa, O. Ikkala

Title: Hydrogen bonding directed colloidal self-assembly of nanoparticles into 2D crystals, capsids, and supracolloidal assemblies